Polymer 51 (2010) 2661–2667

Contents lists available at ScienceDirect

Polymer

journal homepage: www.elsevier.com/locate/polymer

Hexagonally ordered arrays of metallic nanodots from thin films of functional block copolymers

E. Bhoje Gowd [a,1,*], Bhanu Nandan [a,*], Nadja C. Bigall [b,c], Alexander Eychmüller [b], Petr Formanek [a], Manfred Stamm [a]

[a] Leibniz Institute of Polymer Research Dresden, Hohe Strasse 6, 01069, Dresden, Germany
[b] Physical Chemistry, Technical University of Dresden, Bergstrasse 66b, 01062, Dresden, Germany
[c] Istituto Italiano di Tecnologia, Via Morego 30, 16163 Genoa, Italy

ARTICLE INFO

Article history:
Received 30 December 2009
Received in revised form
12 March 2010
Accepted 28 March 2010
Available online 7 April 2010

Keywords:
Block copolymers
Nanoparticles
Nanostructures

ABSTRACT

We demonstrate a new and simple route to fabricate highly dense arrays of hexagonally close packed inorganic nanodots using functional diblock copolymer (PS-*b*-P4VP) thin films. The deposition of pre-synthesized inorganic nanoparticles selectively into the P4VP domains of PS-*b*-P4VP thin films, followed by removal of the polymer, led to highly ordered metallic patterns identical to the order of the starting thin film. Examples of Au, Pt and Pd nanodot arrays are presented. The affinity of the different metal nanoparticles towards P4VP chains is also understood by extending this approach to PS-*b*-P4VP micellar thin films. The procedure used here is simple, eco-friendly, and compatible with the existing silicon-based technology. Also the method could be applied to various other block copolymer morphologies for generating 1-dimensional (1D) and 2-dimensional (2D) structures.

1. Introduction

Nanometer scale patterning of surfaces has attracted a great attention from interdisciplinary scientists as it has applications ranging from electronics to biomedicine. Several methods are known for nanometer scale patterning including electron beam lithography, X-ray lithography, optical lithography, and imprint lithography [1–8]. However, a feature size less than 30 nm in a large area is hard to achieve with the above-mentioned lithography techniques. Therefore, the scientific and industrial community is searching for simple patterning approaches in order to tackle the challenge to generate feature sizes less than 30 nm. Block copolymer based nanofabrication is an emerging approach for the production of nanostructured materials due to the unrelenting reduction in feature sizes on integrated circuitry [9–11]. Block copolymers readily self-assemble to form a variety of nanoscale periodic patterns including spheres, cylinders, and lamellae with typical dimensions of 5–50 nm [12–19]. The optimal utilization of phase-separated block copolymer thin films involves several steps, i.e. working with appropriate film thickness, controlling orientation and lateral ordering of the microdomains, and elimination or surface reconstruction of the minor component to obtain ordered arrays of nanopores [13–15,17]. Thus obtained block copolymer templates were exploited to achieve secondary patterns of interest by further treatment with a variety of different methods including chemical and physical vapor deposition, electrodeposition, incorporation of metal nanoparticles, and chemical reduction techniques [18–27].

The controlled incorporation of nanoparticles into self-assembled block copolymers has attracted a great deal of interest as this process is simple and does not need external fields for depositing nanoparticles into the block copolymer domains [18,24–50]. Moreover, it is an efficient way for improving the properties of materials at the nanometer scale. The stabilization of these nanoparticles in order to prevent them from aggregation and their controlled spatial arrangement in an ordered fashion on a substrate is a challenging problem of today. A number of methods have been developed to selectively incorporate metallic nanoparticles into the desired block copolymer domains. These methods either used pre-loading or post-loading of nanoparticles or inorganic salts into block copolymer domains followed by additional process steps. Pre-loading implies that the block copolymer solution is loaded with nanoparticles or inorganic salts and then deposited onto the surface, while post-loading implies that the loading with nanoparticles or inorganic salts takes place after the formation of the thin film/nanotemplates. In pre-loading, the pre-synthesized

* Corresponding authors. Fax: +49 (0351) 4658 281.
E-mail addresses: gowd@ipc.iisc.ernet.in, bhojegowd@yahoo.com (E.B. Gowd), nandan@ipfdd.de (B. Nandan).
[1] Present address: Department of Inorganic and Physical Chemistry, Indian Institute of Science, Bangalore, India.

0032-3861/$ – see front matter © 2010 Elsevier Ltd. All rights reserved.
doi:10.1016/j.polymer.2010.03.049

metallic nanoparticles of the desired size, shape, and surface chemistry are mixed with block copolymer solution to produce nanopatterned block copolymer-supported arrays. In this approach the metallic nanoparticles have been modified in such a way that they selectively favor solubilization in one block of the polymer [32–34]. This approach exploits enthalpic interactions between the block copolymer and the functionalized nanoparticle surfaces to achieve precise particle placement. Post-loading has the advantage that the deposition and the loading steps are independent of each other. The periodicity of the original structure is preserved in the final nanoparticle array. In this method, block copolymer micelles or templates were used as the nanocompartments to load the defined amount of metal precursor/nanoparticles [36,40–43]. Among the post-loading methods, those using nanoporous block copolymer templates are the potentially most interesting ones, because such approaches are simple and can be easily extended to yield large area samples. For example, Russell and co-workers have utilized polystyrene-*block*-poly(methyl methacrylate) (PS-*b*-PMMA) based nanotemplates for the deposition of CdSe nanoparticles, where the lateral distribution of the nanoparticles into the nanopores was manipulated by physical forces such as capillary forces or electric fields [44,45]. More recently, our group used switchable polystyrene-*block*-poly(4-vinyl pyridine) (PS-*b*-P4VP) block copolymer templates for the deposition of pre-synthesized palladium nanoparticles [46]. In this method, the lateral arrangement of the nanoparticles inside the pores of the templates was manipulated by the preferential interaction of the nanoparticles with the P4VP chains which are available at the pore walls. However, these approaches still have limitations in terms of the complexity of fabrication steps and precise particle placement.

Herein, a new and simple route to fabricate hexagonally close packed inorganic nanodots using functional diblock copolymer (PS-*b*-P4VP) thin films is described. The deposition of pre-synthesized inorganic nanoparticles selectively into the P4VP domains of PS-*b*-P4VP thin films, followed by removal of the polymer, led to highly ordered metallic patterns identical to the order of the starting thin film. Moreover, changing the chain length or volume fraction of the P4VP block allowed us to control the size and the distance between the arrays of nanodots. The affinity of the different metal nanoparticles towards P4VP chains was also understood by extending this approach to PS-*b*-P4VP micellar thin films. Examples of Au, Pt and Pd nanodot arrays are presented. This general method may be used to fabricate ultrahigh-density nanostructures (that is, having areal densities in excess of 10 terabits per square inch).

2. Experimental section

2.1. Synthesis of nanoparticles

Procedures similar to the synthesis route described by Brown et al. [57] were used to synthesize Au, Pt and Pd nanoparticles with average particle diameter of 3.5 ± 0.5 nm, 2.5 ± 0.5 nm and 3.8 ± 0.5 nm. The precursors used for the synthesis of the metal nanoparticles were aqueous solutions of tetrachloroaureate (99.9%, Sigma–Aldrich), chloroplatinic acid (ACS reagent, Sigma–Aldrich) and tetrachloropalladate synthesized by dissolving palladium(II) chloride (99.999%, Sigma–Aldrich) in hydrochloric acid in the molecular ratio $PdCl_2$:HCl 1:2, dissolving with deionized water and filtering with a 0.22 μm PVDF syringe filter.

In a typical synthesis, to a flask with deionized water 0.27 mmol of the metal precursor were added. After 1 min 11 mL of an aqueous solution of 1% sodium citrate were added. Another 30 s later, 5.5 mL of a freshly prepared (in the case of gold nanoparticles ice-cold) 0.08% sodium borohydride and 1% sodium citrate solution in deionized water were quickly injected. The resulting volume in the flask was 500 mL. After a reaction time of 10 min the solution is cooled down to room temperature. If macroscopic contaminations were present (mainly in the case of palladium nanoparticle solutions), they were separated using a hydrophilic syringe filter.

2.2. Block copolymer thin film preparation

Three kinds of PS-*b*-P4VP with different M_n were purchased from Polymer Source, Inc. and used without further purification. PS-*b*-P4VP with M_n = 40.9 kg/mol (M_n^{PS} = 32.9 kg/mol; M_n^{P4VP} = 8.0 kg/mol) and a polydispersity of 1.06, and PS-*b*-P4VP with M_n = 59.0 kg/mol (M_n^{PS} = 41.5 kg/mol; M_n^{P4VP} = 17.5 kg/mol) and a polydispersity of 1.07 were dissolved in chloroform to obtain a 1 wt% polymer solution. The polymer solutions were filtered three times through Millipore 0.2 μm Teflon filters. Thin films were prepared by dip-coating at a speed of 1.0 mms^{-1} onto silicon wafers, which were cleaned with dichloromethane in an ultrasonic bath for 20 min followed by further cleaning in a 1:1:1 mixture of 29% ammonium hydroxide, 30% hydrogen peroxide, and deionized water for 1.5 h at 65 °C. The films were exposed to 1,4-dioxane vapours for 2 days in a sealed glass chamber. The chamber was opened to allow the solvent to evaporate freely once an approximate swelling ratio of 2.75 was reached in the BC thin film. The BC thin films were dipped into the as-prepared aqueous solution of nanoparticles for 2 h. After removal, the thin films were repetitively washed with deionised water in order to ensure the complete removal of any non-adsorbed or weakly adsorbed nanoparticles. The nanoparticle-deposited thin films were then cross-linked using a 254 nm germicidal UV lamp (type G8T5, 2.5 W, *TecWest, Inc.*, U.S.A.) briefly before the pyrolysis, to avoid the flow of polymer at high temperature. The polymer was removed by pyrolysis in an air furnace at 450 °C for 2 h. On the other hand, PS-*b*-P4VP copolymer molecular weight of 39.0 kg/mol (M_n^{PS} = 20.0 kg/mol; M_n^{P4VP} = 19.0 kg/mol and polydispersity of 1.09) was dissolved in toluene at 70 °C for 2 h to yield a 1 wt% polymer solution. The micelles were dip-coated onto a silicon substrate as mentioned above. These micelles were further annealed in toluene vapors for 8 h to improve the long-range order. Metallic nanodots were obtained using the same procedure as discussed above for thin films. Scanning force microscopy (Digital Instruments, Inc., Santa Barbara) (SFM) imaging was performed using a Dimension 3100 and a CP microscope (Park Scientific Instrument, Inc.) in the tapping mode. High resolution scanning electron microscopy (HRSEM) was performed using a Zeiss Ultra 55 Gemini scanning electron microscope with an acceleration voltage of 5 kV. TEM was performed using a FEI CM 200 transmission electron microscope at an accelerating voltage of 200 kV. The samples for TEM were prepared by floating the polymer film in a 1 M aq. NaOH solution and transferring the film onto a TEM grid with a holey carbon film. The film thickness was measured by ellipsometry (SENTECH Instruments GmbH, Germany). XPS experiments were performed with an

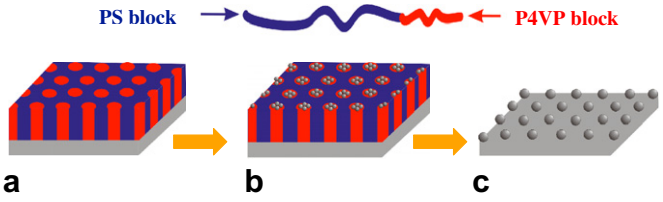

Fig. 1. Schematic sketch of the fabrication process. (a) PS-*b*-P4VP thin film with P4VP cylinders aligned perpendicular to the surface. (b) PS-*b*-P4VP thin film after the nanoparticle deposition. Nanoparticles selectively decorated the swollen P4VP block. (c) Hexagonally close packed inorganic nanodots remain on the silicon substrate after polymer removal.

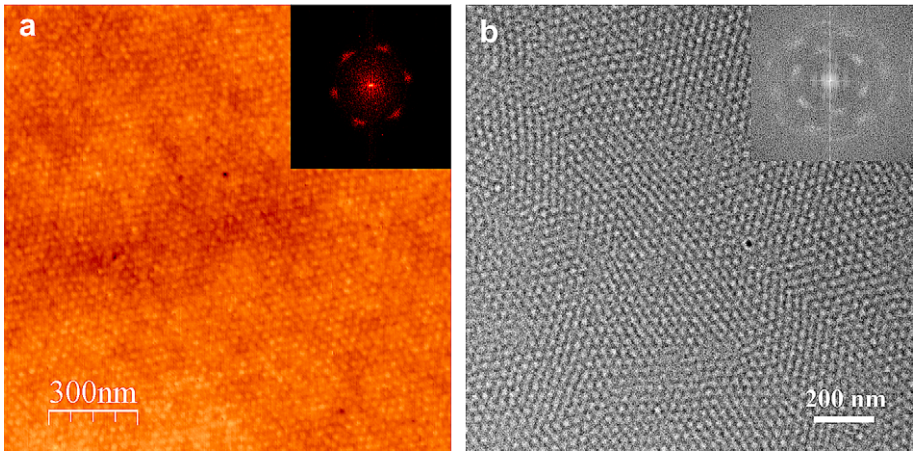

Fig. 2. Highly ordered PS-*b*-P4VP thin film with close packed P4VP cylinders in a PS matrix (center-to-center distance: 29 ± 2 nm). (a) SFM height image (b) TEM image (intentionally defocused to increase the image contrast). The inset shows a fast Fourier transform image to show the long-range order.

AXISULTRA spectrometer (Kratos Analytical, U.K.) equipped with a monochromatized Al Kα X-ray source of 300 W at 20 mA.

3. Results and discussion

The fabrication process of hexagonally close packed inorganic nanodots using a block copolymer (BC) thin film is illustrated in Fig. 1. A cylinder forming block copolymer PS-*b*-P4VP was used to make arrays of nanoscaled dots. PS-*b*-P4VP has excellent microdomain ordering properties due to its large Flory–Huggins interaction parameter compared to the other commonly used block copolymers. An essentially disordered 28 ± 2 nm thick PS-*b*-P4VP thin film was deposited onto the silicon substrate by dip-coating and then annealed in saturated vapors of 1,4-dioxane to obtain an equilibrium microdomain morphology consisting of close packed P4VP cylinders in a PS matrix (Fig. 1a). By immersing the BC thin film into simple aqueous solutions of inorganic nanoparticles, the P4VP chains preferentially attracted the nanoparticles, while the PS matrix remained unaltered (Fig. 1b). The resulting hybrid thin films were stabilized under UV-irradiation, and subsequent pyrolysis at 450 °C or oxygen plasma etching removed the cross-linked block copolymer films completely leaving well-defined arrays of inorganic nanodots (Fig. 1c) on the silicon substrate. The detailed patterning mechanism is discussed below.

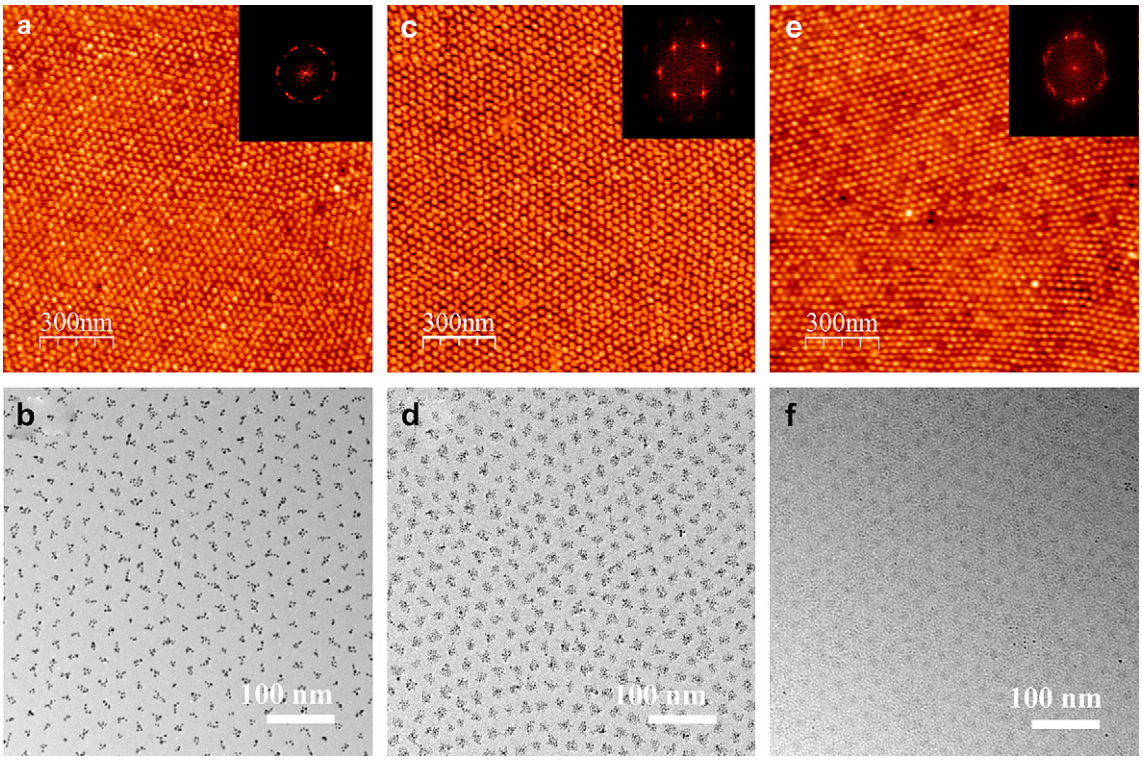

Fig. 3. PS-b-P4VP thin films after the deposition of Au, Pt and Pd nanoparticles from their respective aqueous solutions. The nanoparticles are selectively deposited on P4VP domains in all the films. (a, b) SFM and TEM images, respectively, of the Au deposited film. (c, d) SFM and TEM images, respectively, of the Pt deposited film. (e, f) SFM and TEM images, respectively, of the Pd deposited film. Note: The palladium nanoparticles were not observed in the TEM image as they were washed away during film etching in NaOH solution for TEM measurements due to weaker interaction of Pd with P4VP chains. The inset shows a fast Fourier transform image to show the long-range order.

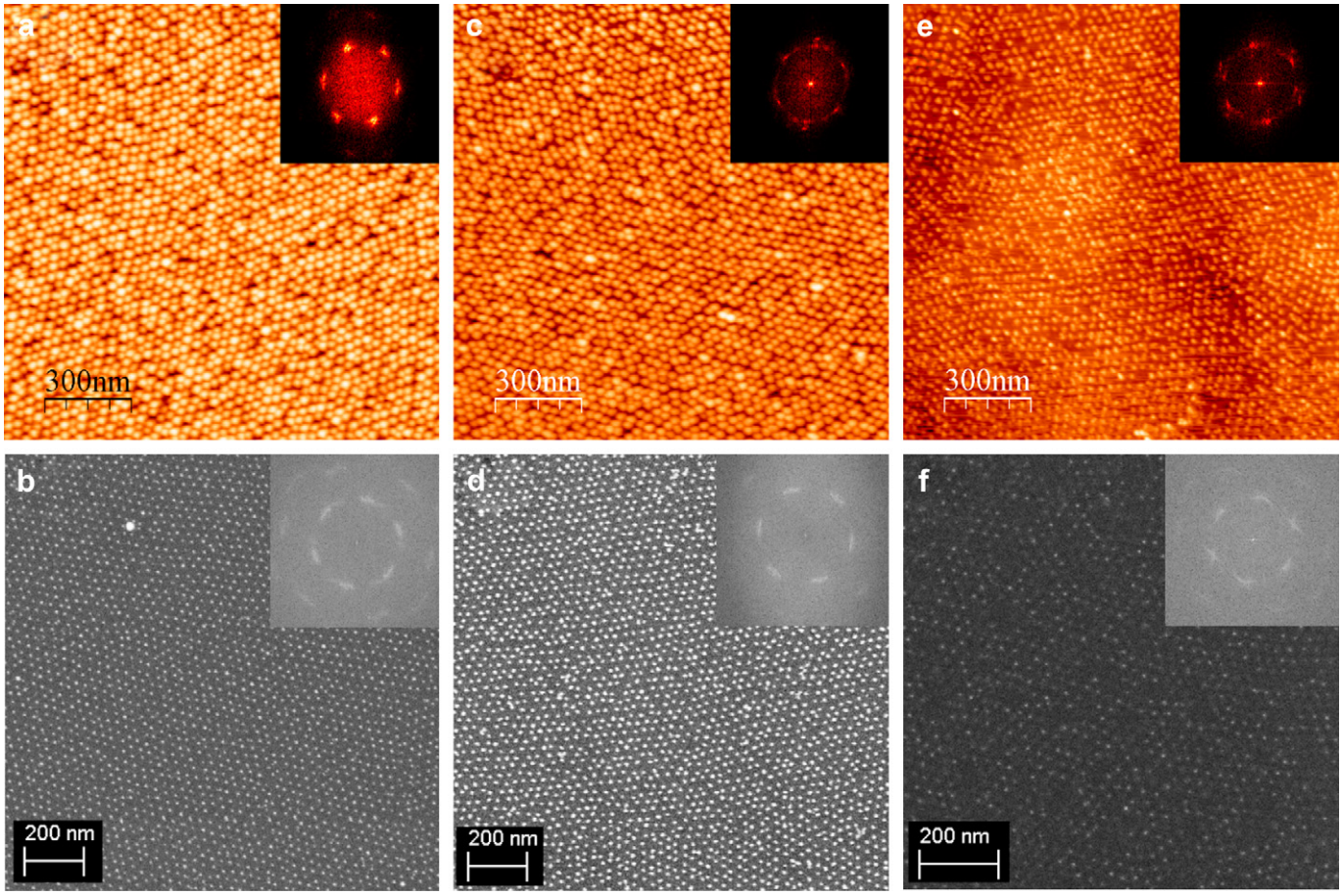

Fig. 4. SFM (top) and SEM (bottom) images of inorganic nanodots with a center-to-center distance of 29 ± 2 nm on silicon substrates after the removal of polymer thin film. (a, b) Au nanodots (c, d) Pt nanodots (e, f) Pd nanodots. The inset shows a FFT image to show the long-range order.

Block copolymer thin films were prepared by dip-coating process using 1 wt% PS-*b*-P4VP (M_n^{PS} = 32.9 kg/mol; M_n^{P4VP} = 8.0 kg/mol) chloroform solution onto silicon wafers. Fig. 2 shows the height-mode scanning force microscopy (SFM) and transmission electron microscopy (TEM) images of PS-*b*-P4VP film (thickness: 28 ± 2 nm) after solvent vapor annealing and subsequent drying. The film directly deposited from chloroform solution showed a disordered worm-like pattern due to fast solvent evaporation, leaving the chains not enough time to attain equilibrium morphology. These films were further annealed in saturated vapors of 1,4-dioxane to obtain the highly oriented arrays of hexagonally packed cylindrical microdomains oriented normal to the substrate. The brighter and darker areas in both the images show the P4VP cylindrical microdomains and the PS matrix, respectively. The fast Fourier transformation (FFT) of Fig. 2a showed six sharp first order reflections clearly indicating that the cylindrical domains of the P4VP are packed in a hexagonal lattice. The average diameter of the P4VP cylinders is 15 ± 1 nm with an average center-to-center distance between adjacent cylinders of 29 ± 2 nm. On the other hand, the FFT of Fig. 2b showed six-point pattern with second order, which may be due to relatively small focused area compared to that of SFM image. It is also worth mentioning here that the 1 M NaOH solution used for floating the films for TEM measurements did not disturb the long-range order of PS-*b*-P4VP films.

PS-*b*-P4VP thin films were then immersed into aqueous solutions of pre-synthesized Au, Pt and Pd nanoparticles at ambient conditions. The nanoparticles were stabilized by negatively charged citrate ions. TEM revealed the mean particle diameter of Au, Pt and Pd nanoparticles to be 3.5 ± 0.5 nm, 2.5 ± 0.5 nm, and 3.8 ± 0.5 nm, respectively. After 2 h of incubation, thin films were removed from the nanoparticles solution and were washed repetitively with deionized water in order to ensure the complete removal of the non-adsorbed or weakly adsorbed nanoparticles. Fig. 3 shows the SFM and TEM images of the PS-*b*-P4VP thin films after the deposition of Au, Pt and Pd nanoparticles. As demonstrated by SFM (Fig. 3a, c and e), incubation of the thin films in aqueous solutions of nanoparticles resulted in selective deposition of the nanoparticles almost exclusively to the P4VP domains. The nanoparticles deposition on the surface exactly mirrors the surface morphology of the starting thin film and the lateral order was retained perfectly as confirmed from the FFT pattern. To verify the number of nanoparticles deposited on each P4VP domain and to avoid the SFM tip size limitations in determining the particle size, we further imaged the samples using TEM. Films were etched from the silicon wafer using 1 M NaOH solution. Lower magnification TEM images (see Supporting Information, Fig. S1) also showed that the lateral order persisted over an area of 2 × 2 μm^2 scale in all the samples. Fig. 3b shows the Au nanoparticles, which are deposited uniformly and almost exclusively on the P4VP domains. No contrast difference is observed between the PS matrix and P4VP cylindrical domains, whereas the nanoparticles are clearly visible on the surface of polymer thin film. Higher magnification TEM images (not shown here) allowed us to estimate the average number of Au nanoparticles deposited on each P4VP domain (5 ± 1). The preferential interaction between Au and P4VP is mainly responsible for binding of nanoparticles exclusively on top of the P4VP and such interaction is well-studied [51–53].

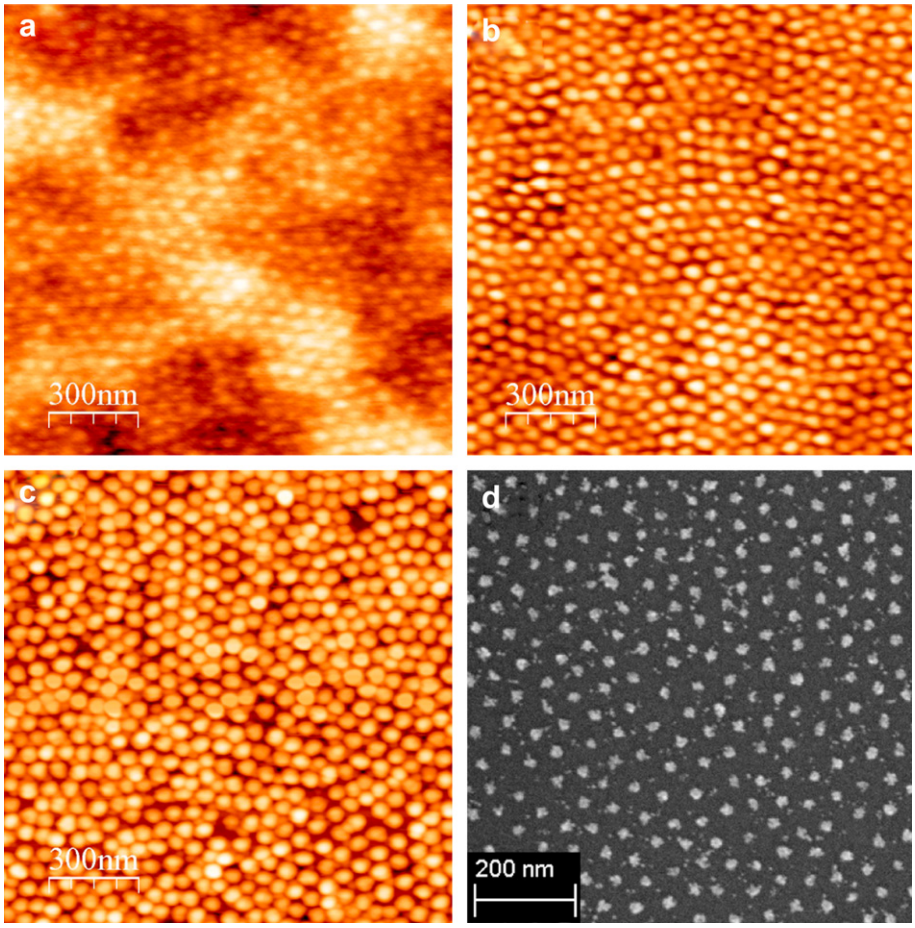

Fig. 5. Height-mode SFM images of (a) PS-b-P4VP thin film with close packed P4VP cylinders in a PS matrix (center-to-center distance: 56 ± 1 nm), (b) the PS-b-P4VP thin film after the deposition of Pt nanoparticles from aqueous solution, and (c) hexagonally packed Pt nandots with a center-to-center distance of 56 ± 1 nm after the polymer removal. (d) SEM image of the same sample shown in (c).

Similar results were obtained with the Pt nanoparticles as shown in Fig. 3d. However, the average number of Pt nanoparticles deposited on each P4VP domain is 15 ± 2, which is due to the smaller size of Pt nanoparticles used here. On the other hand, no Pd nanoparticles were observed in TEM image shown in Fig. 3f, even though, the corresponding SFM image showed patches of Pd on P4VP domains. This means that the weakly adsorbed Pd nanoparticles were probably removed from the P4VP domains during the film etching in the presence of 1 M NaOH solution. These results suggest that metals used here have different affinity towards P4VP. In order to further confirm such difference in affinity between P4VP chains and metal nanoparticles, we used PS-*b*-P4VP miceller thin films, where P4VP chains (core) are buried within a uniform layer of polystyrene (corona) and details will be discussed below.

In the next step, the polymer thin film was removed either by oxygen plasma etching or by pyrolysis in air at 450 °C, to leave behind arrays of metallic nanodots on the surface of the silicon substrate. It is worth mentioning here that a stabilization of the polymer film by cross-linking was crucial before exposing it to pyrolysis or oxygen plasma. In the case of non-cross-linked thin films, the nanoparticles tend to aggregate because of the mobility of polymer chains at higher temperature (above glass transition temperature) during pyrolysis [46]. In this work, the cross-linking of the polymer thin film was done using UV-irradiation to avoid segmental mobility of the polymer chains during pyrolysis. Fig. 4 shows the SFM and high resolution scanning electron microscopy (HRSEM) images of highly ordered arrays of metallic nanodots on silicon. The HRSEM images almost look similar to the SFM images, albeit the difference in sizes of the nanodots, which is due to SFM tip surface convolution effects [54]. It is also worth mentioning that by the plasma treatment or pyrolysis the nanoparticles agglomerate within each domain to a single nanodot as seen in the HRSEM images. In all cases, the hexagonal packing (insets of Fig. 4) and the average center-to-center spacing of 29 ± 2 nm were perfectly maintained even after the polymer removal and are identical to that of the original thin film. The average heights of the resulting Au, Pt and Pd nanodots were measured to be 6 ± 1, 6 ± 1.5, and 3.5 ± 0.5 nm, respectively, as obtained from the SFM section profiles (see Supporting information, Fig. S2), and the average breadths of the nanodots were measured from HRSEM to be 15 ± 2, 16 ± 2, and 3.8 ± 0.5 nm, respectively. Even though the PS-*b*-P4VP used for the deposition of Au, Pt and Pd had the same molecular weight, the average sizes of the different metallic nanodots are different, which may be again attributed to the difference in the affinity between the metallic species and the P4VP (the details will be discussed below). XPS was used to show that the nanodot structures obtained were indeed those of Au, Pt and Pd. XPS spectra of the Pt and Pd nanodots obtained after polymer removal are shown as examples (see Supporting Information, Fig. S3) and the positions of the XPS peaks observed were at the same binding energy values as before the template removal [55].

To vary the separation distance and diameter of the cylindrical domains, a different molecular weight PS-*b*-P4VP was chosen with M_n^{PS} = 41.5 kg/mol; M_n^{P4VP} = 17.5 kg/mol. This block copolymer

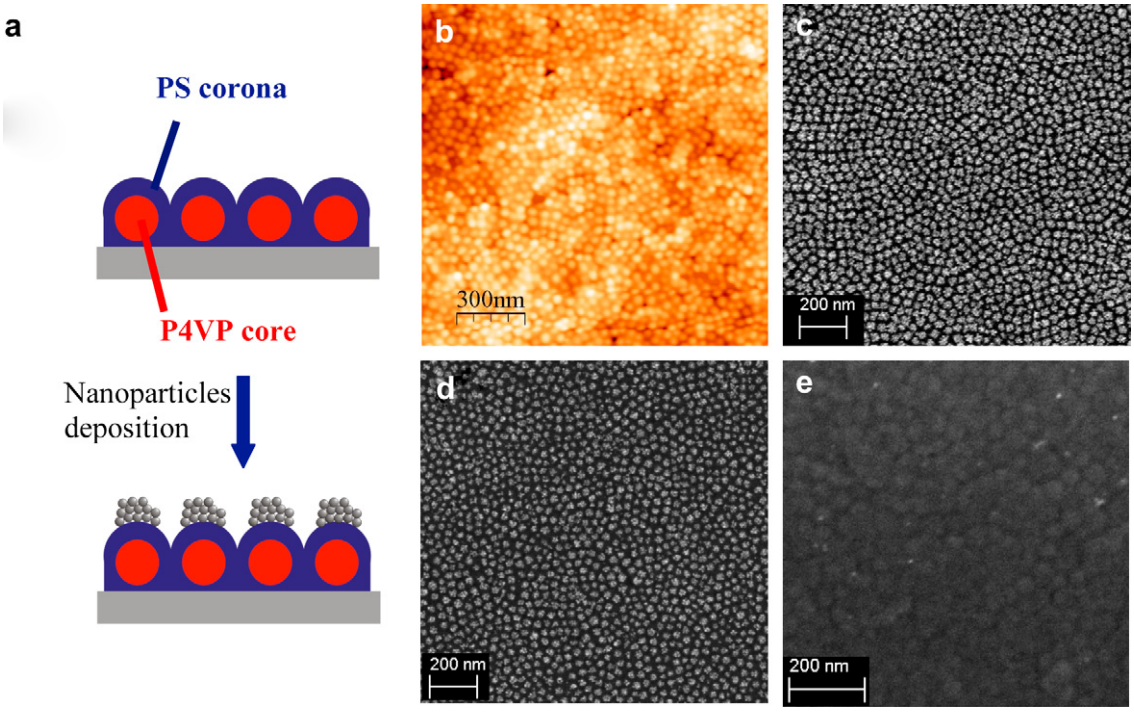

Fig. 6. (a) Schematic diagram of inorganic nanoparticles deposited onto dried micelles. (b) SFM image of PS-b-P4VP dried micelles on a silicon substrate with a center-to-center spacing of 55 ± 2 nm. SEM images of micelles after the deposition of (c) Au, (d) Pt, and (e) Pd nanoparticles. Note: The palladium nanoparticles were not deposited onto the micelles due to weaker interactions between the palladium and the P4VP chains surrounded by the PS barrier.

composition also provides hexagonally packed cylinders with an average center-to-center spacing of 56 ± 2 nm and an average diameter of the P4VP cylinders of ~26 ± 2 nm. In the same manner as discussed above, exemplarily the fabrication of Pt nanodots was demonstrated. Fig. 5 shows SFM images of the PS-b-P4VP thin film before and after the deposition of the Pt nanoparticles and the corresponding SFM and HRSEM images of Pt nanodots after the removal of the polymer. As expected, the average center-to-center spacing and the average size of the nanodots increased with increasing molecular weight and volume fractions of PS and P4VP. These results suggest that by changing the volume fraction or chain length of P4VP, one could tune the density of the nanoparticles deposited on the domains and ultimately adjust the final size of the nanodots. The methodology described here could be utilized to obtain arrays of nanodots with high areal density and lowest possible feature sizes up to 10 nm simply by selecting the appropriate starting molecular weights of PS and P4VP blocks and appropriate starting diameter of the nanoparticles.

As discussed in the preceding, we investigated the interaction between P4VP chains and metal nanoparticles by extending the fabrication approach to micellar morphologies. Here the PS block forms a corona around a P4VP core and acts as a barrier to avoid the direct contact between P4VP and the nanoparticles. For that purpose, PS-*b*-P4VP copolymer having a molecular weight of 39.0 kg/mol (M_n^{PS} = 20.0 kg/mol; M_n^{P4VP} = 19.0 kg/mol) and polydispersity of 1.09 was dissolved in toluene, a selective solvent for PS. The dip-coated film shows micelles on the surface and these micelles were further annealed in saturated vapours of toluene to improve the long-range order. Fig. 6 shows a schematic diagram of the nanoparticle deposition on micelle thin films along with various microscopy images before and after the deposition of the nanoparticles. Fig. 6b shows the SFM height image of micellar thin films after solvent vapour annealing in toluene. PS blocks form a corona around a core of the less soluble P4VP block to reduce energetically unfavourable interactions with the solvent [56]. These micelles were used for the deposition of nanoparticles and the procedure is the same as discussed above. Fig. 6c–d show HRSEM images of the PS-*b*-P4VP micelle thin films after the deposition of Au, Pt and Pd nanoparticles. The Au and Pt nanoparticles were densely deposited on the PS corona exactly on the top of the buried P4VP core, whereas no Pd deposition was found. These results suggest that the surfaces of Au and Pt have stronger affinity towards the P4VP chains than that of Pd. A similar observation was made in the preceding section using PS-*b*-P4VP thin films. More recently, we fabricated ordered arrays of Pd nanodots using the PS-*b*-P4VP based nanotemplates, where the P4VP chains are readily available at the pore walls to attract the Pd nanoparticles [46]. When we extended this pore-filling method to Pt and Au nanoparticles, a large number of nanoparticles was deposited onto the surface of the block copolymer template (see Supporting Information, Fig. S4), due to the strong affinity of these nanoparticles with the P4VP chains, which are available at the pore walls of the nanotemplate. From these observations, we may say that the affinity between the metal and the P4VP is crucial in selecting the deposition method. The methodology described here is very different from the previously reported methods, where the majority of the researchers prepared metallic nanostructures by direct complexation of inorganic salt precursors to one of the block copolymer domain, followed by conversion of the inorganic precursor to a nanoparticle [38–43]. In addition, the method described here is simple and can be extended to other morphologies like spheres, in-plane oriented cylinders, and lamellas to generate 1D and 2D structures.

4. Conclusions

In summary, we have demonstrated a very simple, general, and efficient route to generate nanoscopic arrays of ordered inorganic nanodots with controlled feature sizes up to 26 nm using functional block copolymer thin films. We have fabricated arrays of noble-metal nanodots (Au, Pt and Pd), which are of substantial interest for

various scientific and industrial applications due to their unique optical, electronic and catalytic applications [58,59]. The results obtained here allow us to understand the difference in the affinity of metal surfaces to P4VP chains. We conclude that by the described method it is feasible to obtain arrays of nanodots with possible feature sizes down to 10 nm simply by selecting the appropriate molecular weights of PS and P4VP blocks. The methodology reported here is fast, highly substrate-independent, and the usage of aqueous solutions of nanoparticles for nanofabrication further makes this process less toxic. Furthermore, this method could be applied to various morphologies for generating 1D and 2D structures, as well as to different kinds of nanoparticles e.g. from magnetic or semiconducting materials.

Acknowledgements

E.B.G. is grateful to the Alexander von Humboldt foundation for a research fellowship. The authors thank Dr. Paul Simon for TEM and Dr. Frank Simon for XPS measurements. This research was supported by the priority program of Deutsche Forschungsgemeinschaft (SPP1165, Project No. STA324/31) as well as the project STABILIGHT and the NoE PHOREMOST within the framework program 6 of the European Union.

Appendix. Supporting information

Supplementary data associated with this article can be found in the online version, at doi:10.1016/j.polymer.2010.03.049.

References

[1] Bratton D, Yang D, Dai J, Ober CK. Polym Adv Technol 2006;17:94.
[2] Gates BD, Xu Q, Stewart M, Ryan D, Willson CG, Whitesides GM. Chem Rev 2005;105:1171.
[3] Ito T, Okazaki S. Nature 2000;406:1027.
[4] Chou SY, Keimel C, Gu J. Nature 2002;417:835.
[5] Kim SO, Solak HH, Stoykovich MP, Ferrier NJ, de Pablo JJ, Nealey PF. Nature 2003;424:411.
[6] Craighead HG. Science 2000;290:1532.
[7] Guo LJ. Adv Mater 2007;19:495.
[8] Bhushan B. Springer handbook of nanotechnology. Heidelberg, Germany: Springer; 2004.
[9] Whitesides GM, Kriebel JK, Mayers BT. In: Huck WTS, editor. Nanoscale assembly, vol 9. USA, Ch: Springer; 2005.
[10] Hamley IW. Angew Chem Int Ed 2003;42:1692.
[11] Whitesides GM, Mathias JP, Sato CT. Science 1991;254:1312.
[12] Krishnamoorthy S, Hinderling C, Heinzelmann H. Mater Today 2006;9:40.
[13] Li M, Ober CK. Mater Today 2006;9:30.
[14] Xu T, Stevens J, Villa J, Goldbach JT, Guarini KW, Black CT, et al. Adv Funct Mater 2003;13:698.
[15] Park S, Wang JY, Kim B, Xu J, Russell TP. ACS Nano 2008;2:766.
[16] Mansky P, Harrison CK, Chaikin PM, Register RA, Yao N. Appl Phys Lett 1996;68:2586.
[17] Thurn-Albrecht T, Steiner R, DeRouchey J, Stafford CM, Huang E, Bal M, et al. Adv Mater 2000;12:787.
[18] Minelli C, Hinderling C, Heinzelmann H, Pugin R, Liley M. Langmuir 2005;21:7080.
[19] Lopes WA, Jaeger HM. Nature 2001;414:735.
[20] Thurn-Albrecht T, Schotter J, Kastle GA, Emley N, Shibauchi T, Krusin-Elbaum L, et al. Science 2000;290:2126.
[21] Crossland EJW, Ludwigs S, Hillmyer MA, Steiner U. Soft Matter 2007;3:94.
[22] Sidorenko A, Tokarev I, Minko S, Stamm MJ. Am Chem Soc 2003;125:12211.
[23] Darling SB, Yufa NA, Cisse AL, Bader SD, Sibener SJ. Adv MCter 2005;17:2446.
[24] Segalman RA. Mater Sci Eng R 2005;48:191.
[25] Darling SB. Prog Polym Sci 2007;32:1152.
[26] Ansari IA, Hamley IW. J Mater Chem 2003;13:2412.
[27] Kim DH, Kim SH, Lavery K, Russell TP. Nano Lett. 2004;4:1841.
[28] Boontongkong Y, Cohen RE. Macromolecules 2002;35:3647.
[29] Glass R, Möller M, Spatz JP. Nantotechnology 2003;14:1153.
[30] Haryono A, Binder WH. Small 2006;2:600.
[31] Spatz JP, Herzog T, Mößmer S, Ziemann P, Möller M. Adv Mat 1999;11:149.
[32] Thompson RB, Ginzburg VV, Matsen MW, Balazs AC. Science 2001;292:2469.
[33] Thompson RB, Ginzburg VV, Matsen MW, Balazs AC. Macromolecules 2002;35:1060.
[34] Kim BJ, Chiu JJ, Yi G, Pine DJ, Kramer EJ. Adv Mater 2005;17:2618.
[35] Chiu JJ, Kim BJ, Kramer EJ, Pine DJ. J Am Chem Soc 2005;127:5036.
[36] Spatz JP, Mößmer S, Hartmann C, Möller M, Herzog T, Krieger M, et al. Langmuir 2000;16:407.
[37] Spatz JP, Chan VZH, Mössmer S, Kamm F, Plettl A, Ziemann P, et al. Adv Mat 2002;14:1827.
[38] Spatz JP, Roescher A, Möller M. Adv Mat 1996;8:337.
[39] Spatz JP, Roescher A, Sheiko S, Krausch G, Möller M. Adv Mat 1995;7:731.
[40] Lohmueller T, Bock E, Spatz JP. Adv Mat 2008;20:2297.
[41] Kästle G, Boyen H-G, Weigl F, Lengl G, Herzog Th, Ziemann P, et al. Adv Funct Mater 2003;13:853.
[42] Chai J, Buriak JM. ACS Nano 2008;2:489.
[43] Chai J, Wang D, Fan X, Buriak JM. Nat Nanotech 2007;2:500.
[44] Misner MJ, Skaff H, Emrick T, Russell TP. Adv Mat 2003;15:221.
[45] Zhang Q, Xu T, Butterfield D, Misner MJ, Ryu DY, Emrick T, et al. Nano Lett. 2005;5:357.
[46] (a) Nandan B, Gowd EB, Bigall NC, Eychmüller A, Formanek P, Simon P, et al. Adv Funct Mater 2009;19:2805;
(b) Gowd EB, Nandan B, Vyas MK, Bigall NC, Eychmüller A, Schlorb H, et al. Nanotechnology 2009;20:415302.
[47] Hamley IW. Nanotechnology 2003;14:R39.
[48] Tsutsumi K, Funaki Y, Hirokawa Y, Hashimoto T. Langmuir 1999;15:5200.
[49] Lazzari M, Lopez-Quintela MA. Adv Mat 2003;15:1583.
[50] Lin Y, Böker A, He J, Sill K, Xiang H, Abetz C, et al. Nature 2005;434:55.
[51] Park S, Wang JY, Kim B, Russell TP. Nano Letters 2008;8:1667.
[52] Kunz MS, Shull KR, Kellock AJ. J Colloid Interface Sci. 1993;156:240.
[53] Shull KR, Kellock AJ. J Poly Sci Polym Phys 1995;33:1417.
[54] Grabar KC, Brown KR, Keating CD, Stranick SJ, Tang SL, Natan MJ. Anal Chem 1997;69:471.
[55] Moulder JF, Stickle WF, Sobol PE, Bomben KD. In: Chastain J, editor. Handbook of X-ray photoelectron spectroscopy. Perkin–Elmer Corporation Eden Prairie Minnesota; 1984.
[56] Riess G. Prog Polym Sci. 2003;28:1107.
[57] Brown KR, Walter DG, Natan MJ. Chem Mater 2000;12:306.
[58] Kreibig U, Vollmer M. Optical properties of metal clusters, vol 25. Heidelberg: Springer; 1995.
[59] Takagi D, Homma Y, Hibino H, Suzuki S, Kobayashi Y. Nano Lett 2006;6:2642.